14 Aug 2019

Comparison of Fatigue Performance between Additively Manufactured and Wrought 304L Stainless Steel using a Novel Fatigue Test Setup

M. M. Parvez

Y. Chen

Joseph William Newkirk
Missouri University of Science and Technology, jnewkirk@mst.edu

Frank W. Liou
Missouri University of Science and Technology, liou@mst.edu

Recommended Citation

M. M. Parvez et al., "Comparison of Fatigue Performance between Additively Manufactured and Wrought 304L Stainless Steel using a Novel Fatigue Test Setup," *Proceedings of the 30th Annual International Solid Freeform Fabrication Symposium (2019, Austin, TX)*, pp. 353-363, University of Texas at Austin, Aug 2019.

Solid Freeform Fabrication 2019: Proceedings of the 30th Annual International
Solid Freeform Fabrication Symposium – An Additive Manufacturing Conference
Reviewed Paper

COMPARISON OF FATIGUE PERFORMANCE BETWEEN ADDITIVELY MANUFACTURED AND WROUGHT 304L STAINLESS STEEL USING A NOVEL FATIGUE TEST SETUP

M. M. Parvez*, Y. Chen*, J. W. Newkirk†, F. F. Liou*

*Department of Mechanical and Aerospace Engineering, Missouri University of Science and Technology, Rolla, MO 65401, USA

†Department of Materials Science and Engineering, Missouri University of Science and Technology, Rolla, MO 65401, USA

Abstract

In this research, a novel adaptive controlled fatigue testing machine was designed for bending type high cycle fatigue test. A unique dual gauge section Krouse type mini specimen was designed for simply supported transverse bending. Displacement controlled fatigue tests were implemented using an electromechanical actuator. The variation in the control signal and load observed during the test provides unique insights into realizing the deterioration of the specimen due to fatigue. These analyses were utilized to compare the fatigue performance of wrought and additively manufactured 304L stainless steel. The influence of the build direction on fatigue performance was also investigated by testing specimens with 0, 45, and 90 degrees build direction. These comparisons were carried out at different levels of displacement amplitude.

Introduction

Additive manufacturing (AM) is a process of joining materials into a 3D part layer by layer from 3D computer data, which is opposite to the traditional manufacturing process of using subtractive method [2]. Due to the additive approach, AM has some advantages when compared with subtractive manufacturing. AM process can fabricate complex 3D structures, reduce the lead time, and improve the efficiency of raw materials [3]. During the past decade, AM has been studied in various types of materials, including metals, polymers, glass, ceramics, and composite materials. As metals and their alloys are of great importance in day to day life, AM of metals has become popular in recent years, in which austenitic stainless steel is widely used in various industrial fields. Selective laser melting (SLM) is one of the AM methods used in the field of metal AM [4]. The mechanical properties characterization of austenitic stainless steel using SLM has attracted a lot of interest. Alsalla [5] reported the tensile and yield strength of SLM-processed 316L stainless steel are higher than cast materials, while the elongation is relatively weaker because of the porosity generated due to the gas pore or lack-of-fusion. Yusuf et al. [6] reported the hardness in SLM 316L stainless steel was higher than wrought parts. Casati et al. [7] studied the microstructure of SLM 316L stainless steel. Both columnar and equiaxial grains were formed which is different from traditional 316L stainless steel. Montero [8] investigated the effect of heat treatment on SLM 316L stainless steel. Since most of the mechanical failures of structures are due to fatigue, the fatigue testing study is indispensable in failure mechanism analysis. Fatigue properties of several popular metal alloys made by SLM such as Ti-6Al-4V [9], 15-5PH [10], AlSi10Mg [11], and Inconel 718 [12] have been investigated.

In this study, we compared the fatigue performance of additively manufactured 304 stainless steel material built at different orientation with wrought bulk material. A novel displacement-controlled fatigue testing method was implemented to conduct fully reversed (R = -1) bending fatigue test on mini specimens since axial loading tests on mini specimens suffer buckling. During both monotonic and cyclic loading test, mini specimens are preferred in AM material's mechanical properties characterization due to the high cost of manufacturing and specimen preparation [13]. But mini specimens exhibit a higher mechanical strength including fatigue compared to the standard specimens [14-19] because standard specimens have greater risk volume to contain larger defects what lead to crack growth resulting in fatigue failure [20-26]. Nonlinear stress distribution in bending type test is another reason for mini specimens to demonstrate higher fatigue strength [27, 28]. But for the comparative study of fatigue performance, mini specimens were used in this study. To obtain a constant stress distribution within the gauge section, a Krouse type specimen with a dual gauge section was designed for simply supported loading. The dual gauge section increases the risk volume and maintains one-dimensional loading. The specimen was designed for simply supported loading because at a given load, the displacement is four times the displacement in a fully clamped loading. We also designed and implemented nonstandard testing equipment for the displacement-controlled test to reduce the cost since standard testing equipment is very expensive [29]. The designed test equipment also consumes less electrical power because of the tests performed on mini specimens require a smaller range of loads.

During the displacement-controlled fatigue test, the applied load decreases with the decrease in the stiffness of the material. As the load decreases, the control signal decreases as well. The change in the control signal provides a unique insight into realizing the deterioration of the material in terms of the nucleation and propagation stage. Extended studies have been carried out to develop techniques to identify the nucleation and propagation phase [29-35]. In this research, we introduced a control signal monitoring (CSM) method to identify the phases. This method was applied to compare the fatigue performance of SLM fabricated and wrought 304 SS material.

Experimental Setup

A dual gauge section Krouse type mini specimen was designed in this research work. Figure 1 illustrates the drawing of the wedge-shaped specimen. The specimen is clamped at both ends with line contacts for simply supported loading. The length of the specimen between both clamping ends is 1 inch, while the total gauge length is approximately one-third of the effective length. The advantage of using dual gauge is the load distributed symmetrically along with the gauges. The fatigue failure can occur randomly at any gauge. Moreover, the dual gauge section covers a large surface area with increased volume to capture all different types of surface and microstructural defects. The common defects in AM materials are void, pores, microcracks, and lack of fusion. AM materials have a higher probability of defects compared to wrought materials. A sensitivity and uncertainty analysis was also performed to determine the optimal thickness (0.65 mm) of the specimen since mini specimen needs strict dimensional tolerances. In summary, the specimen was specially designed for fatigue testing of additive manufacturing materials. The designed specimen type, size, and loading mechanism add a novelty to the current study.

The test materials used in this study are hot rolled and annealed 304 bulk material, and SLM fabricated bars of 304L stainless steel powders. The chemical composition of both the wrought material and powder is listed in Table 1. From the chemistry of both materials, the

wrought material may be characterized as 304 SS, and the powder as 304L SS due to its low content of interstitial, N, C, O, etc. The relatively close chemistry of materials may add a better understanding of the comparative study though the weight percentage of Ni is 2% higher in the powder but not expected to make a significant difference in test results. In the SLM process, a laser beam was applied on the powder bed of a Renishaw AM250 machine to selectively melt and join a layer of powder particles. Once a raster pattern layer was finished, the next layer was fabricated with 67^0 rotation angles. Finally, the steel bars were fabricated layer by layer using a set of optimized parameters listed in Table 2 to yield maximum part density. Fine surfaced finished (average Ra = 0.482 μm, average Rz = 4.242 μm) specimens were prepared using a wired electric discharge machine (W-EDM); so the effect of surface roughness on initiating the crack would be minimal and the failure would occur only due to the presence of major defects within the volume. A schematic representation of the SLM specimens (not in scale) prepared at different build direction is shown in Figure 2.

Mini specimens require a lower range of loads. A low power subwoofer with soft mechanical suspension was used in this study as an actuator since the mathematical modeling of a subwoofer is relatively similar to an electromagnetic actuator. To accommodate the actuator with the test bench, the dust cap of the voice coil was replaced with a lightweight plastic flange. A load cell installed inline between the central clamp and the flange measures the tensile and compressive force. A laser displacement sensor was fixed with a guide rail to measure the displacement at high speed. Figure 3 illustrates a specimen installed on the fatigue test bench for simply supported loading. The specimen is clamped at the center with a surface contact (3 mm × 7 mm), while at both ends the specimen is in line contact with the bearings. Bearing minimizes frictions during the test. Spacers were accommodated between top and bottom of the bearing adapters at both ends to ensure no preload on the specimen. Toggle clamps were used at both clamping ends. Implementing a microcontroller, the measured displacement data were processed to calculate the mean and amplitude of the displacement. The load values were logged using a data acquisition card. An adaptive proportional and derivative (PD) controller was implemented to control the amplitude of the displacement. To maintain the desired displacement, the control signal value was sent to a function generator via Ethernet. A linear power amplifier coupled with the function generator drives the actuator. The displacement and control signal amplitudes were stored for the entire fatigue life cycle to monitor the performance of the controller and to analyze the control signal in identifying the nucleation and propagation phases.

Results and Discussions

A fully reversed (R = -1) bending type fatigue test was performed at room temperature on fine finished wrought and AM specimens. The specimens were actuated for closed loop displacement-controlled sinusoidal excitation at 56 Hz test frequency. The occurrence of fatigue failure at a random location within the gauges, as shown in Figure 4, verifies the design effectiveness of the specimen. Figure 5 illustrates the competency of the adaptive PD controller in maintaining the set displacement amplitude. The displacement amplitude goes very high when the final failure occurs. The control signal amplitude decreases until the final failure. Since the stiffness of the specimen reduces as the crack grows, propagates, and final failure occurs, the load to maintain the desired displacement reduces as well. Therefore, the control signal amplitude goes low.

Table 1: Chemistries of the bulk material and powder for additive manufacturing

Material	C	Mn	Si	S	P	Cr	Ni	Cu	Mo	Co	N	O
Wrought	0.023	1.69	0.43	0.020	0.034	18.10	8.02	0.63	0.24	0.15	0.084	-
Powder	0.015	1.40	0.63	0.004	0.012	18.50	9.90	<0.1	-	-	0.090	0.02

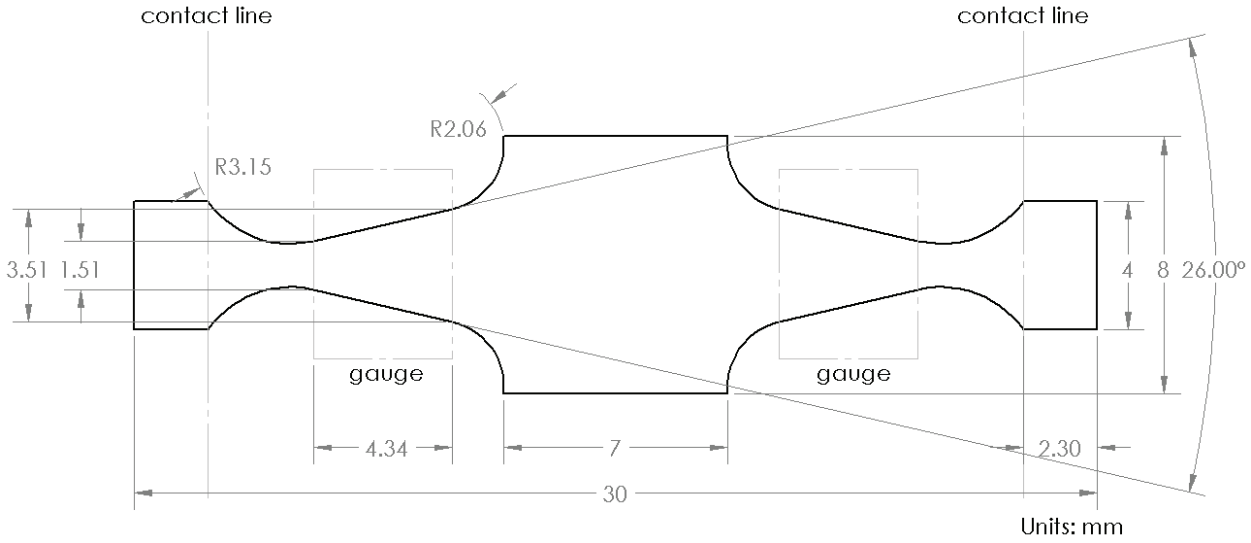

Figure 1: Drawing of the wedge-shaped Krouse type mini specimen showing the dual gauge section, and contact line at both ends for simply supported loading

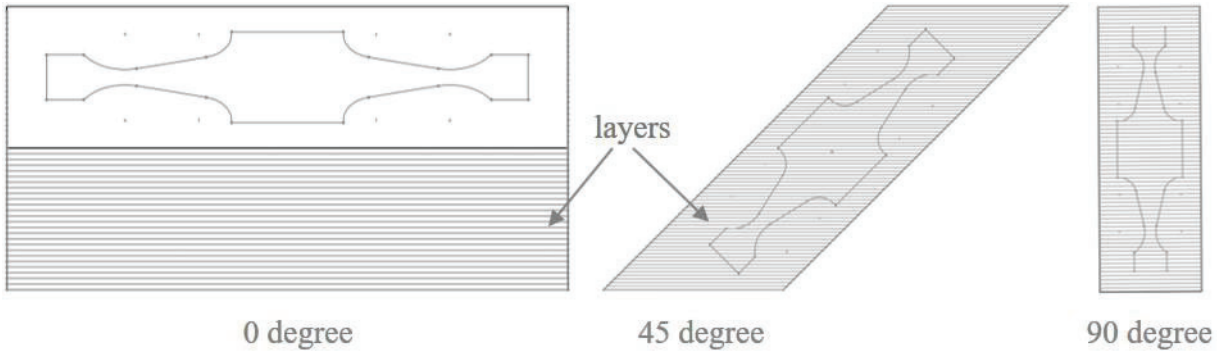

Figure 2: Schematic representation of the specimen cut from SLM parts built at 0^0, 45^0, and 90^0 build orientation

Table 2: Optimized parameters used in the SLM process to fabricate stainless steel bars

Parameter set	Laser power (watt)	Hatch space (μm)	Point distance (μm)	Exposure time (millisecond)	Energy density (MJ/m^3)	Raster rotation (degree)

Nominal	200	85	60	75	58.8	67

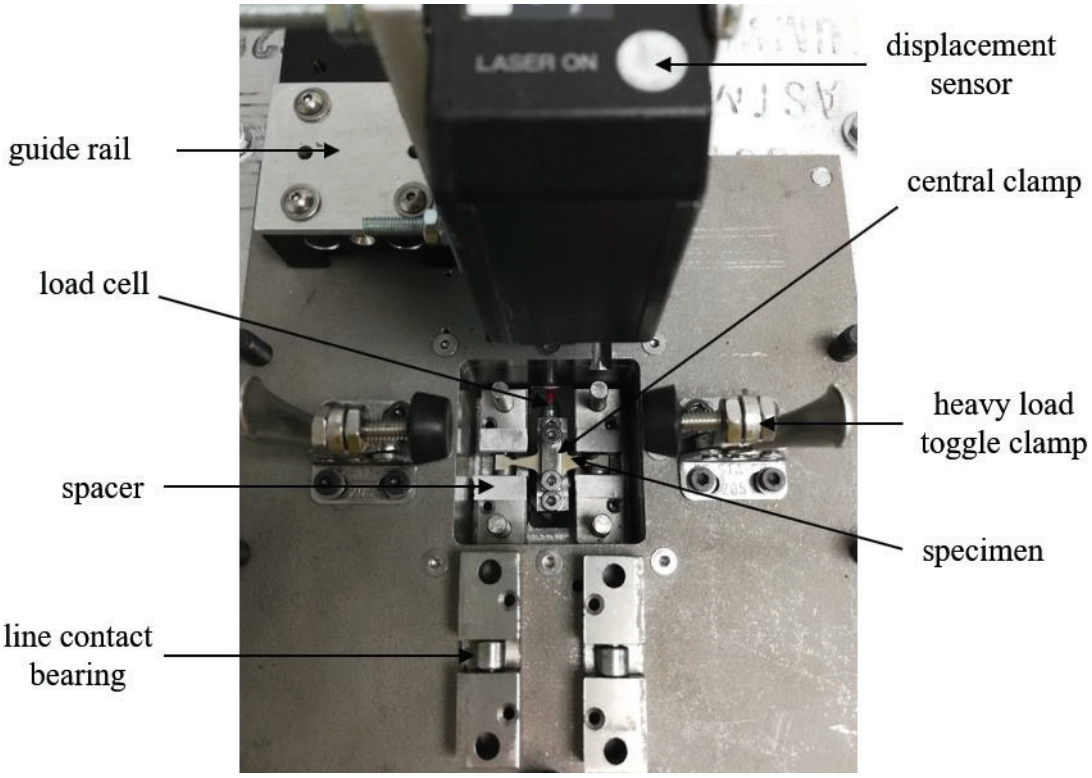

Figure 3: Fatigue testbench setup with simply supported dual gauge section-based specimen

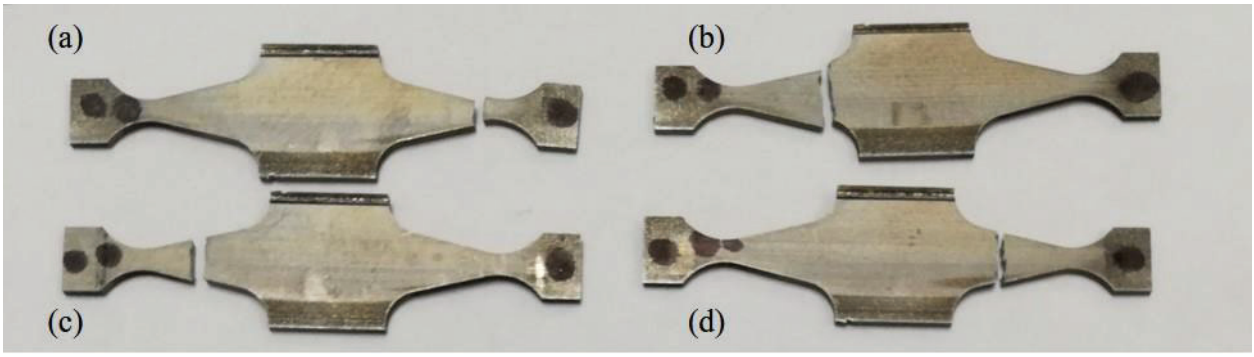

Figure 4: Fatigue failure location of wrought specimens; displacement amplitude, (a): 0.250 mm, (b): 0.275 mm, (c): 0.225 mm, (d): 0.300 mm

In the current work, we implemented a control signal monitoring (CSM) method to identify the nucleation and propagation phase. The stiffness of a material decreases during the nucleation and propagation phase though the rate of the change of the stiffness is different at different phases. Analyzing the control signal, we identified the change in phase from nucleation to propagation. Figure 6 shows the analytical result of the CSM method. Performing a linear regression analysis on the control signal, we estimated the phases. The analysis was applied for all the specimens tested.

To determine the maximum nominal stress on the specimen, the average of the peak load up to the end of nucleation cycle was calculated. The stress in a simply supported bending beam with a central point load is expressed as,

$$\sigma = \frac{M(x)}{I(x)} \frac{h}{2} \tag{1}$$

where, σ, $M(x)$, $I(x)$, and h are the stress, bending moment, second moment of area, and the thickness of the specimen, respectively. For a simply supported beam, $M(x) = \frac{Fx}{2}$, and $M(x) = \frac{b(x)h^3}{12}$, where, F is the force applied, and b is the width of the specimen. In a wedged shaped specimen, $b(x) = 2kx$, where, k is the slope of the shape. The nominal stress can be expressed as,

$$\sigma_{nom} = \frac{3F_{peak}}{2kh^2} \tag{2}$$

Determining the nominal stress, the Wohler curve (S-N plot) was plotted, as shown in Figure 7. SLM fabricated materials are nonhomogeneous and they have a very higher probability of defects (i.e., pores, voids, lack of fusion, inclusion) compared to the wrought materials. Therefore, the SLM fabricated materials regardless of the build direction demonstrate lower fatigue strength (endurance limit: 10^7 cycles) compared to the wrought materials. In comparison to the SLM fabricated materials themselves, the specimens prepared at 0^0 build direction has a higher fatigue strength than the specimens prepared at 45^0, and 90^0 direction. The specimens prepared at 0^0 build direction includes a smaller number of layers at the cross-section than the specimens built in other directions. As a result, the specimens have a lower probability of defects within its volume since a smaller number of layers results in a smaller number of interlayer zones. Interlayer bonding is weak and it has a higher possibility of creating defects during the fabrication of AM materials [30, 31].

For further analysis, the end of nucleation cycle and cycles to failure were plotted for different stress levels. The comparison was done between wrought and SLM fabricated specimens built at 0^0 orientation, and between the SLM fabricated specimens prepared at 45^0, and 90^0 build direction (shown in Figure 8). At all cases, the number of cycles during both the nucleation and propagation cycles increases as the stress value goes low. This validates the SLM fabricated materials follow the conventional phenomena of nucleation and propagation. At the high cycle fatigue, the propagation cycle for the SLM material is less than the propagation of the wrought material. Authors believe that the presence of defects within the volume of the material enhances the propagation rate.

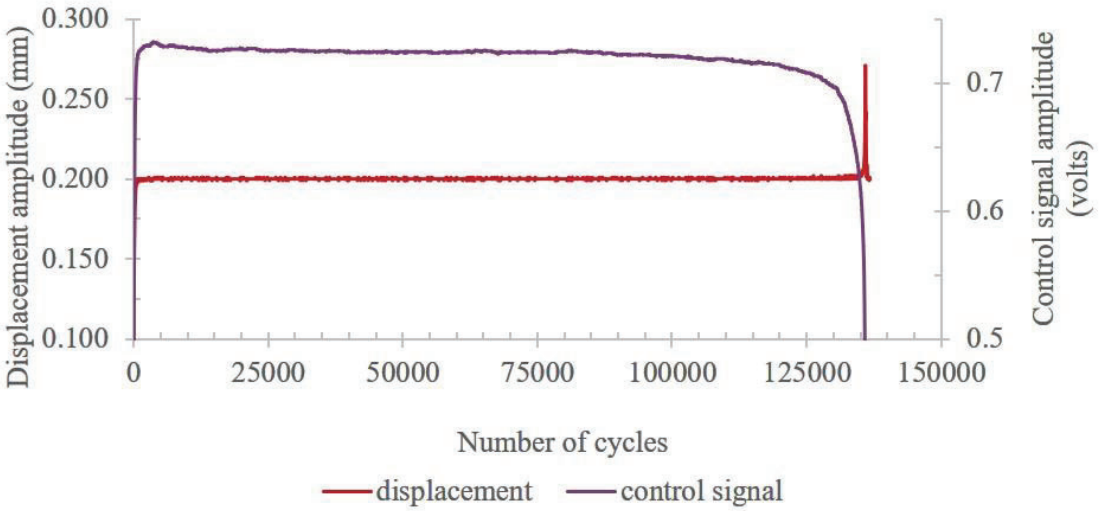

Figure 5: Displacement and control signal amplitude of a wrought specimen displaced at 0.200 mm amplitude

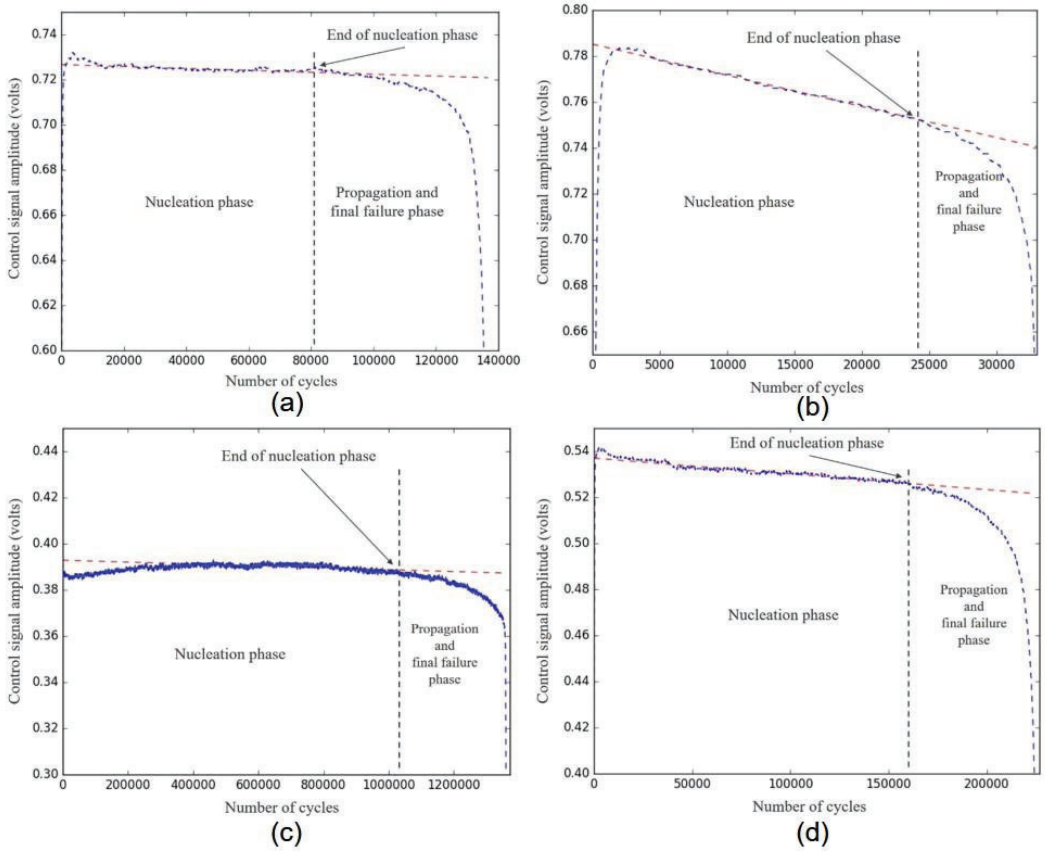

Figure 6: Nucleation and propagation phase, (a): wrought specimen, 0.200 mm displacement amplitude; and SLM fabricated specimen, (b): 0^0 orientation, 0.200 mm displacement amplitude, (c): 45^0 orientation, 0.100 mm displacement amplitude, (d): 90^0 orientation, 0.155 mm displacement amplitude

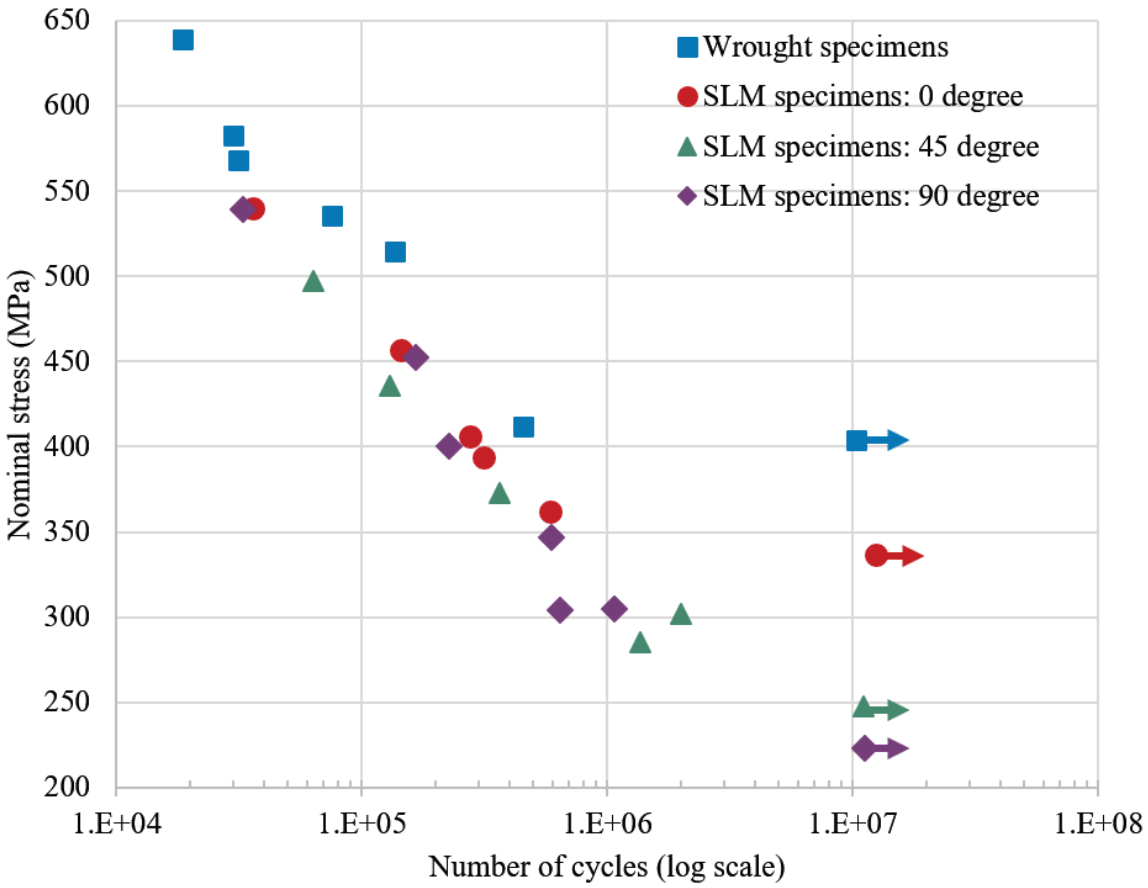

Figure 7: S-N plot of wrought and SLM specimens prepared at different build direction

The loading direction during the fatigue test of the specimens prepared at 0^0 build orientation is normal to the layer direction, while at 45^0, and 90^0 build direction, it is parallel. Therefore, the comparison of the results for 45^0, and 90^0 build orientation is pertinent. As shown in Figure 4, the fatigue crack propagates across the cross-section. A crack must travel through a larger number of layers (illustrated in Figure 2) during both the nucleation and propagation for the specimens built at 45^0 orientation than the specimens at 90^0 orientation. Apart from the presence of defects, this is another reason for the higher number of propagation and nucleation cycle for the specimens built at 45^0 orientation.

Conclusion

In this study, the transverse bending fatigue test was performed on Krouse type mini specimen eliminating the buckling issue with miniature specimen occurred in an axial fatigue test. The dual gauge section captures a large extent of microstructural and surface defects increasing the surface area and volume. The influence of build direction on fatigue performance of SLM fabricated 304L stainless steel was compared applying control signal monitoring method. The analysis illustrates SLM materials demonstrate lower fatigue strength at both nucleation and propagation phase compared to wrought materials. Future studies can include the analysis and comparison of fatigue failure mechanism of additively manufactured 304 stainless steel.

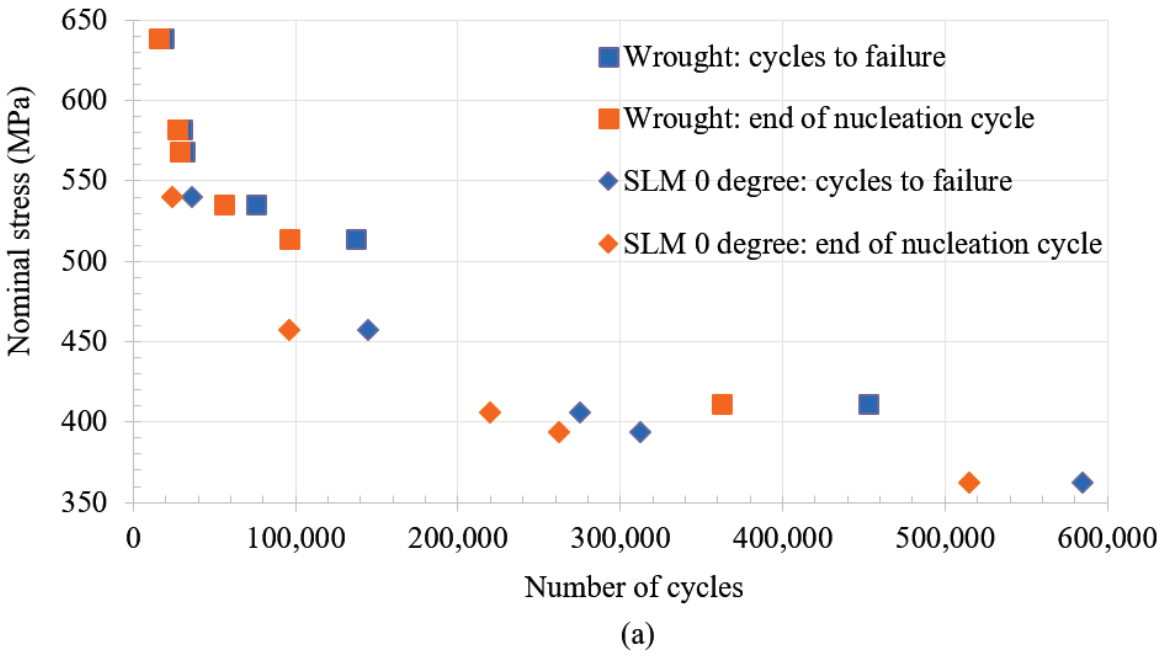

(a)

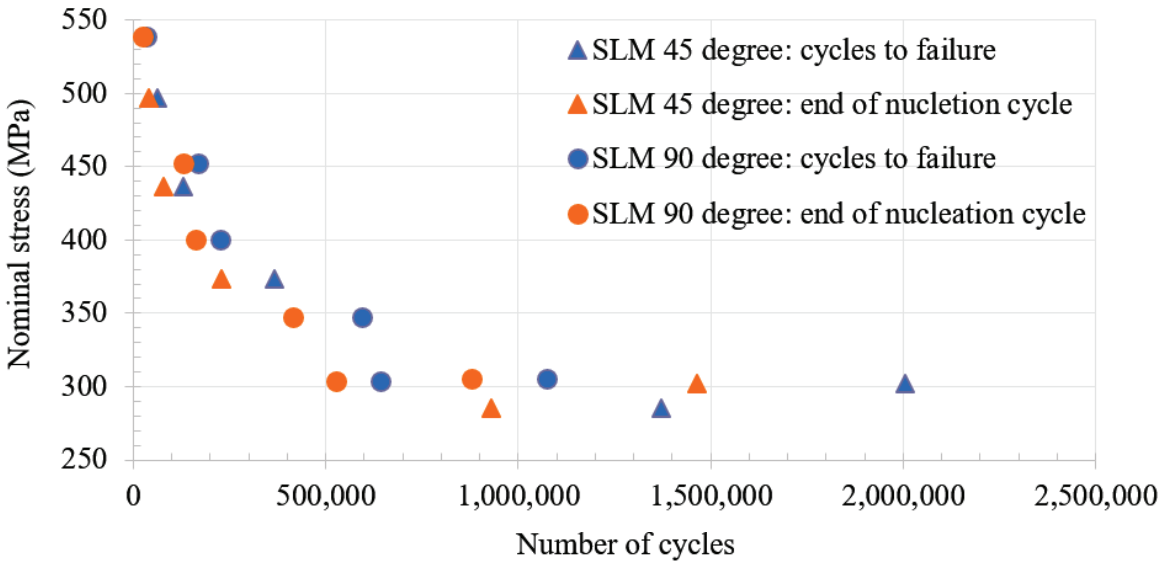

(b)

Figure 8: End of nucleation phase and cycles to failure of (a): wrought specimens and SLM fabricated specimens at 0^0 build orientation, (b): SLM fabricated specimens at 45^0 and 90^0 build orientation

Acknowledgment

This research was supported by National Science Foundation Grant CMMI-1625736. Part of the work was also funded by the Department of Energy's Kansas City National Security Campus which is operated and managed by Honeywell Federal Manufacturing Technologies, LLC under contract number DE-NA0002839.

References

1. Diemar, A., R. Thumser, and J. Bergmann, *Determination of local characteristics for the application of the Weakest-Link Model.* Materialwissenschaft und Werkstofftechnik: Entwicklung, Fertigung, Prüfung, Eigenschaften und Anwendungen technischer Werkstoffe, 2005. **36**(5): p. 204-210.
2. Frazier, W.E., *Metal additive manufacturing: a review.* Journal of Materials Engineering and Performance, 2014. **23**(6): p. 1917-1928.
3. Guo, N. and M.C. Leu, *Additive manufacturing: technology, applications and research needs.* Frontiers of Mechanical Engineering, 2013. **8**(3): p. 215-243.
4. Liu, A., C.K. Chua, and K.F. Leong. *Properties of test coupons fabricated by selective laser melting*. in *Key Engineering Materials*. 2010. Trans Tech Publ.
5. Alsalla, H.H., C. Smith, and L. Hao, *Effect of build orientation on the surface quality, microstructure and mechanical properties of selective laser melting 316L stainless steel.* Rapid Prototyping Journal, 2018. **24**(1): p. 9-17.
6. Yusuf, S., et al., *Investigation on porosity and microhardness of 316L stainless steel fabricated by selective laser melting.* Metals, 2017. **7**(2): p. 64.
7. Casati, R., J. Lemke, and M. Vedani, *Microstructure and fracture behavior of 316L austenitic stainless steel produced by selective laser melting.* Journal of Materials Science & Technology, 2016. **32**(8): p. 738-744.
8. Montero Sistiaga, M., et al. *Effect of heat treatment of 316L stainless steel produced by selective laser melting (SLM)*. in *Proceedings of the 27th Annual International Solid Freeform Fabrication Symposium-An Additive Manufacturing Conference*. 2016.
9. Wycisk, E., et al. *High cycle fatigue (HCF) performance of Ti-6Al-4V alloy processed by selective laser melting*. in *Advanced materials research*. 2013. Trans Tech Publ.
10. Rafi, H.K., T.L. Starr, and B.E. Stucker, *A comparison of the tensile, fatigue, and fracture behavior of Ti–6Al–4V and 15-5 PH stainless steel parts made by selective laser melting.* The International Journal of Advanced Manufacturing Technology, 2013. **69**(5-8): p. 1299-1309.
11. Brandl, E., et al., *Additive manufactured AlSi10Mg samples using Selective Laser Melting (SLM): Microstructure, high cycle fatigue, and fracture behavior.* Materials & Design, 2012. **34**: p. 159-169.
12. Konečná, R., et al., *Microstructure and directional fatigue behavior of Inconel 718 produced by selective laser melting.* Procedia Structural Integrity, 2016. **2**: p. 2381-2388.
13. Karnati, S., et al. *Investigation of tensile properties of bulk and SLM fabricated 304L stainless steel using various gage length specimens*. in *Proceedings of the 27th Annual International Solid Freeform Fabrication Symposium–An Additive Manufacturing Conference*. 2016.
14. Akiniwa, Y., et al., *Notch effect on fatigue strength reduction of bearing steel in the very high cycle regime.* International Journal of Fatigue, 2006. **28**(11): p. 1555-1565.
15. Findley, W., *An explanation of size effect in fatigue of metals.* Journal of Mechanical Engineering Science, 1972. **14**(6): p. 424-428.
16. Leitner, M., et al., *Microporosity and statistical size effect on the fatigue strength of cast aluminium alloys EN AC-45500 and 46200.* Materials Science and Engineering: A, 2017. **707**: p. 567-575.
17. Nakajima, M., et al., *Effect of loading condition on very high cycle fatigue behavior in a high strength steel.* International Journal of Fatigue, 2010. **32**(2): p. 475-480.

18. Wormsen, A., et al., *Non-local stress approach for fatigue assessment based on weakest-link theory and statistics of extremes.* Fatigue & Fracture of Engineering Materials & Structures, 2007. **30**(12): p. 1214-1227.
19. Zhu, S.-P., S. Foletti, and S. Beretta, *Evaluation of size effect on strain-controlled fatigue behavior of a quench and tempered rotor steel: Experimental and numerical study.* Materials Science and Engineering: A, 2018. **735**: p. 423-435.
20. Bažant, Z.P. and D. Novák, *Probabilistic nonlocal theory for quasibrittle fracture initiation and size effect. I: Theory.* Journal of Engineering Mechanics, 2000. **126**(2): p. 166-174.
21. Furuya, Y., *Notable size effects on very high cycle fatigue properties of high-strength steel.* Materials Science and Engineering: A, 2011. **528**(15): p. 5234-5240.
22. Härkegård, G. and G. Halleraker, *Assessment of methods for prediction of notch and size effects at the fatigue limit based on test data by Böhm and Magin.* International Journal of Fatigue, 2010. **32**(10): p. 1701-1709.
23. Lanning, D.B., T. Nicholas, and A. Palazotto, *HCF notch predictions based on weakest-link failure models.* International journal of fatigue, 2003. **25**(9-11): p. 835-841.
24. Lin, H., et al., *Investigation of the Effect of Sample Size on Fatigue Endurance Limit of a Carburized Steel.* SAE Transactions, 2006: p. 525-540.
25. Makkonen, M., *Statistical size effect in the fatigue limit of steel.* International journal of fatigue, 2001. **23**(5): p. 395-402.
26. Sun, C. and Q. Song, *A Method for Predicting the Effects of Specimen Geometry and Loading Condition on Fatigue Strength.* Metals, 2018. **8**(10): p. 811.
27. Lee, Y.-L., et al., *Fatigue testing and analysis: theory and practice*. Vol. 13. 2005: Butterworth-Heinemann.
28. Nakai, Y., et al. *Size effect on fatigue strength of metallic micro-materials*. in *Proceedings of Asian-Pacific Conference on Fracture and Strength*. 1999.
29. Tomaszewski, T. and J. Sempruch. *Verification of the fatigue test method applied with the use of mini specimen*. in *Key Engineering Materials*. 2014. Trans Tech Publ.
30. Olakanmi, E.O., R. Cochrane, and K. Dalgarno, *A review on selective laser sintering/melting (SLS/SLM) of aluminium alloy powders: Processing, microstructure, and properties.* Progress in Materials Science, 2015. **74**: p. 401-477.
31. Zhang, B., Y. Li, and Q. Bai, *Defect formation mechanisms in selective laser melting: a review.* Chinese Journal of Mechanical Engineering, 2017. **30**(3): p. 515-527.